Journal of Biomedical Optics

BiomedicalOptics.SPIEDigitalLibrary.org

Laser-induced microjet injection into preablated skin for more effective transdermal drug delivery

Hun-jae Jang
Eugene Hur
Yoonkwan Kim
Seol-Hoon Lee
Nae G. Kang
Jack J. Yoh

SPIE.

Laser-induced microjet injection into preablated skin for more effective transdermal drug delivery

Hun-jae Jang,[a] Eugene Hur,[b] Yoonkwan Kim,[b] Seol-Hoon Lee,[b] Nae G. Kang,[b] and Jack J. Yoh[a,*]
[a]Seoul National University, Department of Mechanical and Aerospace Engineering, 1 Gwanakro, Gwanakgu, Seoul 151-742, Republic of Korea
[b]LG Household & Health Care R&D Center, 84 Jang-dong, Yuseong-gu, Daejeon 305-343, Republic of Korea

Abstract. A breakthrough in the efficient transdermal delivery of drug via the laser-driven microjet is reported. A single source of laser beam is split into two: one beam ablates a targeted spot on a skin and another beam drives the injector for fast microjet ejection into a preablated spot. This combined ablation and microjet injection scheme using a beam splitter utilizes 1 : 4 laser energy sharing between generation of the microhole via ablation and the microjet which is generated using the Er:YAG laser beam at a 2940-nm wavelength and 150-μs pulse duration. A careful analysis of the injection mechanism is carried out by studying the response of the elastic membrane that separates a driving water unit for bubble expansion from a drug unit for a microjet ejection. The efficiency of the present delivery scheme is evaluated by the abdominal porcine skin test using the fluorescein isothiocyanate staining and the confocal microscopy for quantitative delivery confirmation. The depth of penetration and the injected volume of the drug are also confirmed by polyacrylamide gel tests. [DOI: 10.1117/1.JBO.19.11.118002]

Keywords: drug delivery system; microjet injector; bubble; ablation; beam splitter.

Paper 140384RR received Jun. 16, 2014; accepted for publication Oct. 22, 2014; published online Nov. 18, 2014.

1 Introduction

A drug delivery system based on the microjet has been studied by various researchers.[1–4] Several different mechanisms for generating the microjet include spring, compressed gas, piezoelectric transducer, linear Lorentz force piston, electronic driven bubble, and laser-induced wave or bubble. The introduction of these devices was principally motivated by overcoming needle phobia and contamination from reuse of a conventional needle-based system.[5–1] In the spring or gas-powered devices, it is difficult to control drug dose or jet speed with its piston unit, whereas in the piezoelectric transducer, rather precise control of drug dose was deemed possible. The Lorentz force driven injector has shown a quite reliable performance in comparison to the aforementioned devices. A vapor bubble driven injector for the microjet generation has been proposed in our earlier works,[7,8] where the vapor bubbles are induced by the short pulsed (150 μs) Er:YAG laser beam (2.9 μm) having the best absorptivity in water.

The mechanism of the microjet ejection is as follows: an Er:YAG laser beam is focused inside a driving chamber that is filled with degassed water. An explosive growth of vapor bubble in this chamber gives rise to a sudden deformation of the elastic membrane that separates the drug solution from the driving water. The elastic expansion of the membrane pushes the drug solution and the drug liquid is ejected through the nozzle of a 150-μm diameter. The microjet jet is accelerated to above 100 m/s, which is sufficient for skin penetration and effective delivery of the drug dose. In order to enhance the drug delivery efficiency, 20% of the beam is split into making a microhole in the targeted porcine skin before the microjet of drug solution arrives at the same targeted spot for easier penetration of the outer most layer of the porcine skin.

The skin ablation tests using the Er:YAG laser were reported in the literature. The ablation rate of a normal spiking mode of Er:YAG was considered, and the effect of different pulse durations such as normal-spiking (200 μs) and Q-switched mode (90 ns) was reported by Walsh et al.[9,10] Walsh et al. also investigated conventional thermal damage by varying the laser fluence from 0.5 to 81 J/cm^2. Hibst and Kaufmann[11] studied the optimization of Er:YAG laser parameters for skin ablation and suggested that the crater depth is proportional to the laser fluence. Hohenleutner et al.[12] reported on the effective conditions of thermal ablation and concluded that the thermal damage zone does not increase with the spot size or by the repetition of laser pulses; only the superficial skin is ablated by the Er:YAG laser.

A review of these previous studies on skin ablation using an Er:YAG laser suggests that an Er:YAG laser can be an effective means of ablating the superficial skin layer with minimal thermal damage whereby subsequent microjet injections can be significantly enhanced. In the present study, a combined scheme of skin ablation and microjet injection is used. The drug injection is synchronized by the skin ablation prior to microjet ejection with a time delay between the two processes. A series of high speed camera images are used to investigate the detailed response and responsible mechanism of the laser-based microjet device which makes good use of the elastic membrane and the explosive growth of a large-sized vapor bubble. The rate of expansion for both bubble and membrane is similar, suggesting that the system is optimally designed for efficient transdermal delivery of the drug. Confocal microscopy is used to quantify the depth of drug penetration into a porcine skin treated by fluorescein isothiocyanate (FITC) staining using the present delivery scheme. Furthermore, the penetration process inside the gel is analyzed by using high speed camera images.

*Address all correspondence to: Jack J. Yoh, E-mail: jjyoh@snu.ac.kr

0091-3286/2014/$25.00

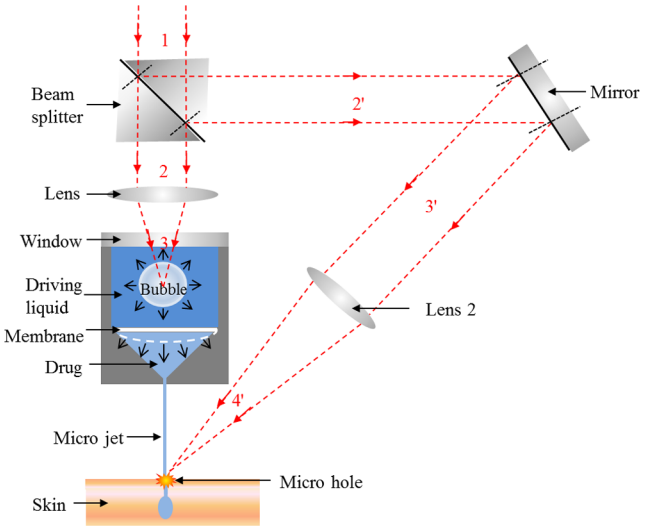

Fig. 1 Schematic of drug delivery with preablation followed by a microjet injection using a beam splitter.

2 Material and Methods

The microjet is generated by a focused Er:YAG laser beam which has a high absorption coefficient in water.[13] The laser used in this study is a custom made laser, built from a standard Er:YAG laser (B&B Systems, Anybeam) for dental procedures. The generated beam from the unit passes through the articulated arm consisting of mirrors until being focused by a lens of 100-mm focal length. The specifications of the laser used in this study are as follows: wavelength is 2940 nm and pulse duration is 150 μs. The bubble is confined by the 11 mm height chamber and the stand-off distance between the center of the lens and the injector top surface is 45 mm. In this experiment, two kinds of studies are conducted. In the first case, the laser beam whose energy is 1085 mJ is focused into a chamber of the injector through the coated sapphire window. Explosive bubble growth occurs as a result of laser beam focusing. The elastic membrane starts to deform due to the sudden pressure rise caused by the bubble expansion. Then the microjet is discharged from the nozzle of 150-μm diameter by the deformation of the membrane. This is referred to as the microjet-only (w/o ablation) case.

The second case is represented in Fig. 1. It makes use of a beam splitter in the preablation–microjet (w/ablation) case. The concept of the combined preablation and microjet ejection is developed in order to increase the efficiency of drug delivery. The laser beam labeled 1 passes through a beam splitter with an 80% transmittance and a 20% reflectance. The transmitted energy of 860 mJ is focused into the driving water in the upper chamber through the sapphire window. The generation of a microjet is identical to the microjet-only case. Now the reflected laser beam denoted as 2′ is reflected by a mirror and then focused into a porcine skin through a lens whose focal length is 100 mm. The expected ablation hole depth and diameter may be inferred from the reference works[9–12] on skin ablation with an Er:YAG laser, which is shown in Table 1. The penetration depth

Table 1 Depth and diameter of the ablation hole on the target skin at given laser fluence.

	Pulse duration	Target	Fluence (J/cm^2)	Depth (μm)	Diameter (μm)
Ablation + microjet (our study)	150 μs	Porcine skin	87	417	679
Walsh et al.[9]	200 μs	Guinea pig skin	50	250	1100
	200 μs	Guinea pig skin	80	400	1100
Walsh et al.[10]	90 ns	Guinea pig skin	25		5 to 10
	200 μs	Guinea pig skin	25		10 to 50
Hibst and Kaufmann[11]	250 μs	Porcine skin	60	320	900
	250 μs	Porcine skin	80	400	900
Hohenleutner et al.[12]	250 μs	Human skin	4	11.2	25 to 100
	250 μs	Human skin	7	15.6	25 to 100

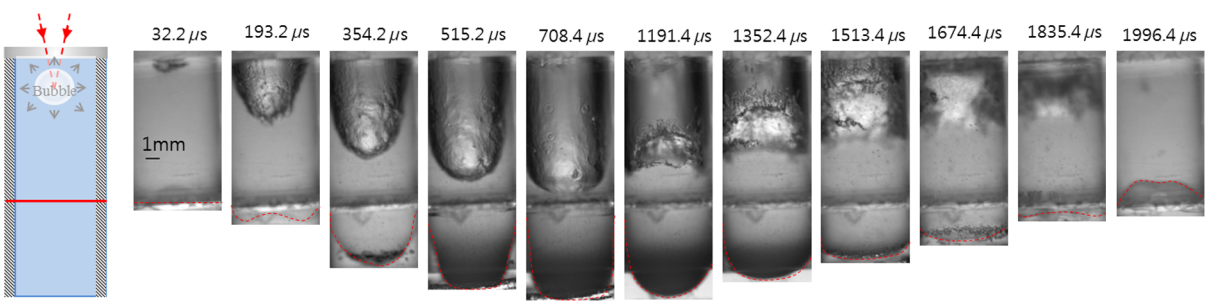

Fig. 2 Sequential images of bubble (upper chamber) and a membrane (dashed line) that separate upper water and lower drug.

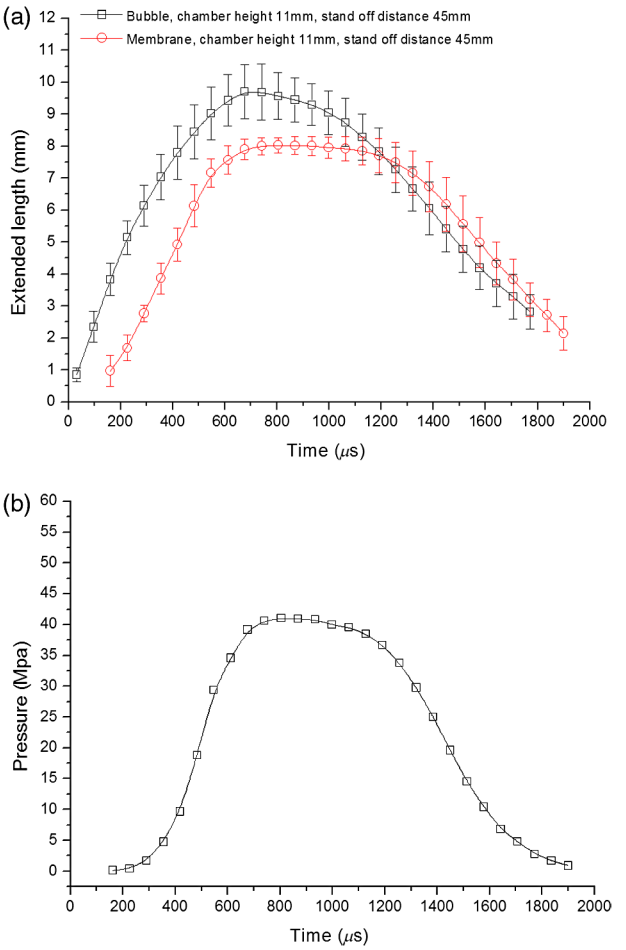

Fig. 3 (a) Extended lengths of bubble and membrane taken from high speed camera images and (b) calculated pressure incurred on thin membrane.

is within 500 μm, and the hole diameter is expected to be larger than the microjet diameter (150 μm). In the present experiment, the laser energy is adjusted to satisfy the target depth and diameter such that the laser fluence of 87 J/cm^2 is used for the present experiment. As for the optimum angle of the ablation beam, we find the angle to be 60 deg from the skin surface. A microhole is created by the preablation scheme, and the hole position is optically aligned with the drug jet impact position. The resulting microjet velocity reached about 69 to 105 m/s.

The bubble behavior, membrane response, and microjet ejection are monitored by the high speed camera images (Phantom V711). The detailed characteristics of bubble, membrane, and microjet are also obtained from the images. The process of a large bubble generation in the driving chamber reveals that its height reaches 11 mm as it is recorded at the rate of 31,007 fps. The deflection of the elastic membrane that separates the drug from water within the injector is also captured by the high speed camera. The resulting microjet ejections are taken at 49,026 fps.

Both penetration experiments using polyacrylamide gel (PAAG) and porcine skin were performed to quantify the depth, width, and injected volume. Black ink is injected into 10%, 20%, and 30% weight ratios of PAAG, and the injected volume is captured by a Nikon camera. Each component of the PAAG is similar to those used in Ref. 14. The process of penetration is also recorded by a high speed camera at 40,000 fps to obtain the instantaneous images of the microjet injections with and without ablations. The penetration experiment on the abdominal porcine skin is also performed. For visualization of the penetration depth within the skin, the injecting liquid is prepared by dissolving 1 g/L of FITC in Dulbecco's phosphate-buffered saline (DPBS). Multiple planar images at specific depths are obtained using confocal microscopy (Zeiss, LSM710). The laser conditions were as follows: 1085 mJ for microjet-only and 1035 mJ for preablation–microjet with 10 Hz for porcine skin and gel.

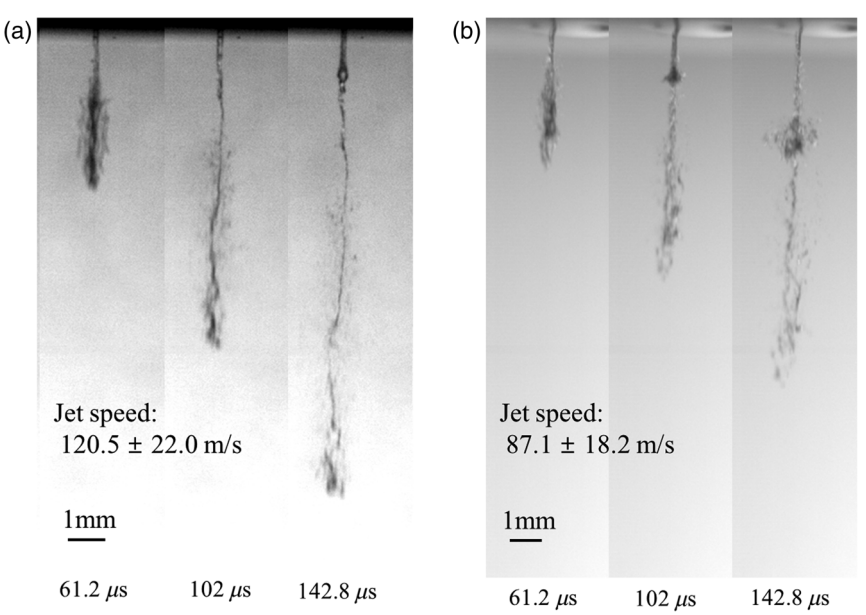

Fig. 4 Sequential images of microjet ejection for (a) microjet-only and (b) preablation–microjet case.

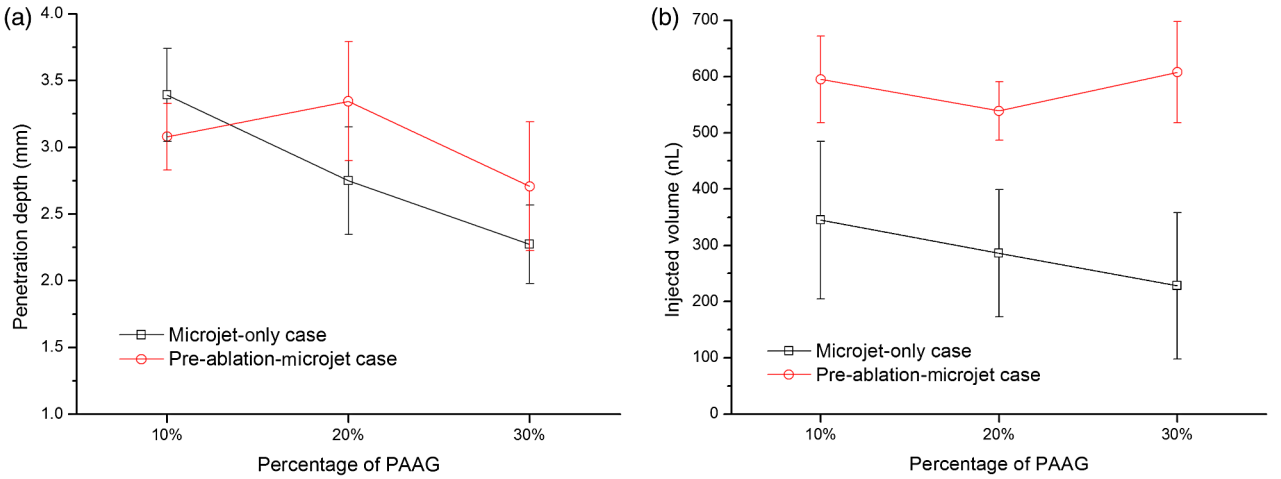

Fig. 5 Penetration parameters [(a) depth and (b) injected volume] for each case.

Table 2 Efficiency parameters (penetration depth and injected volume) of microjet injection are less sensitive to gel strength w/ablation than w/o ablation.

	Penetration depth per energy (mm/J) w/o ablation	Injected volume per energy (μL/J) w/o ablation	Penetration depth per energy (mm/J) w/ ablation	Injected volume per energy (μL/J) w/ ablation
10% PAAG	3.124	0.318	2.974	0.575
20% PAAG	2.534	0.264	3.231	0.521
30% PAAG	2.095	0.220	2.615	0.587

3 Results and Discussion

The typical bubble and membrane motions of the microjet-only case imaged within a transparent injector are carefully studied. Figure 2 shows the sequential images of a stretched bubble and the membrane expansion. The laser beam is focused inside the upper chamber and is separated from a lower drug by a membrane (dashed line). The expansion and collapse of the bubble take place inside the driving water chamber surrounded by an upper window, acrylic cylinder wall, and a silicon rubber membrane at the bottom. One observes the rapid growth of a vapor bubble that becomes fully expanded within the upper chamber. As a result, the membrane is stretched to several millimeters long as shown in this figure. There is a short time elapse between the bubble and the membrane expansion. The maximum stretch by the membrane is attained when a bubble reaches its maximum volume, which is shown at ~708.4 μs. Consequently, the membrane contracts to return to its unstretched position as the bubble collapse takes place.

The dynamics of a membrane are strongly dependent on the bubble expansion. As shown in Fig. 3(a), the growth rate of a bubble and that of a membrane are quite similar. Here, the error bars are representative of the standard deviation across 10 experiments. Also, the rates of decay for both the bubble and membrane are comparable, suggesting that the dynamic response of the confined bubble in the upper chamber and the stretch of the elastic membrane for drug ejection are related to each other.

The membrane deflection is dominated by the pressure loading such that the nonlinear Föppl membrane theory applies.[15] For a thin membrane, the pressure is proportional to the cube of the midpoint deflection of the membrane, which can be estimated by using

$$P = \frac{Eh}{a^4}\left(\frac{w_0}{g(v)}\right)^3, \tag{1}$$

$$g(v) \approx 0.7179 - 0.1706v - 0.1495v^2. \tag{2}$$

Here, $E = 1$ MPa is Young's modulus of the membrane, $h = 0.1$ mm is the membrane thickness, $a = 7$ mm is the

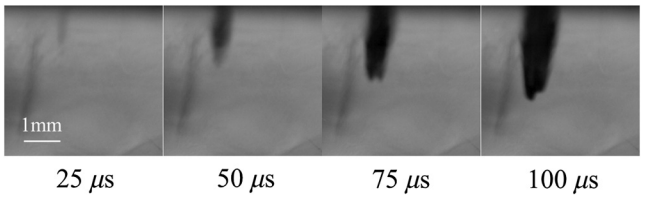

Fig. 6 Microjet-only case: sequential images of penetration of 10% polyacrylamide gel (PAAG) with black ink.

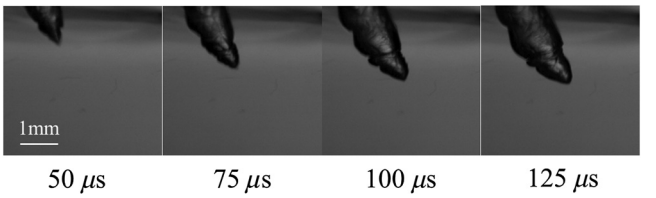

Fig. 7 Preablation–microjet case: sequential images of penetration of 10% PAAG with black ink.

diameter of membrane, w_0 is the midpoint deflection of the membrane obtained from the high speed camera images, $\upsilon = 0.47$ is Poisson's ratio, and $g(\upsilon)$ is calculated as a function of the Poisson's ratio.[15] The stretched lengths of bubble and membrane are obtained from the high speed camera images and presented in Fig. 3(a). The pressure estimation based on this equation is illustrated in Fig. 3(b). The pressure starts to increase rapidly once the bubble expansion begins. There is a time delay between the on-set of bubble expansion and that of pressure rise. A single cycle of growth and collapse is less than 2000 μs, and during that time the pressure eventually reaches its equilibrium.

The microjet as it is discharged from a nozzle of 150-μm diameter is illustrated in Fig. 4. The jet velocity in the microjet-only case is 120.5 ± 22.0 m/s, while in the pre–ablation–microjet case, it is 87.1 ± 18.2 m/s. A relatively slower jet velocity is observed when the laser energy is split 1:4.

A test of three different gel strengths (PAAG 10%, 20%, 30%) is performed as the range of Young's modulus of each

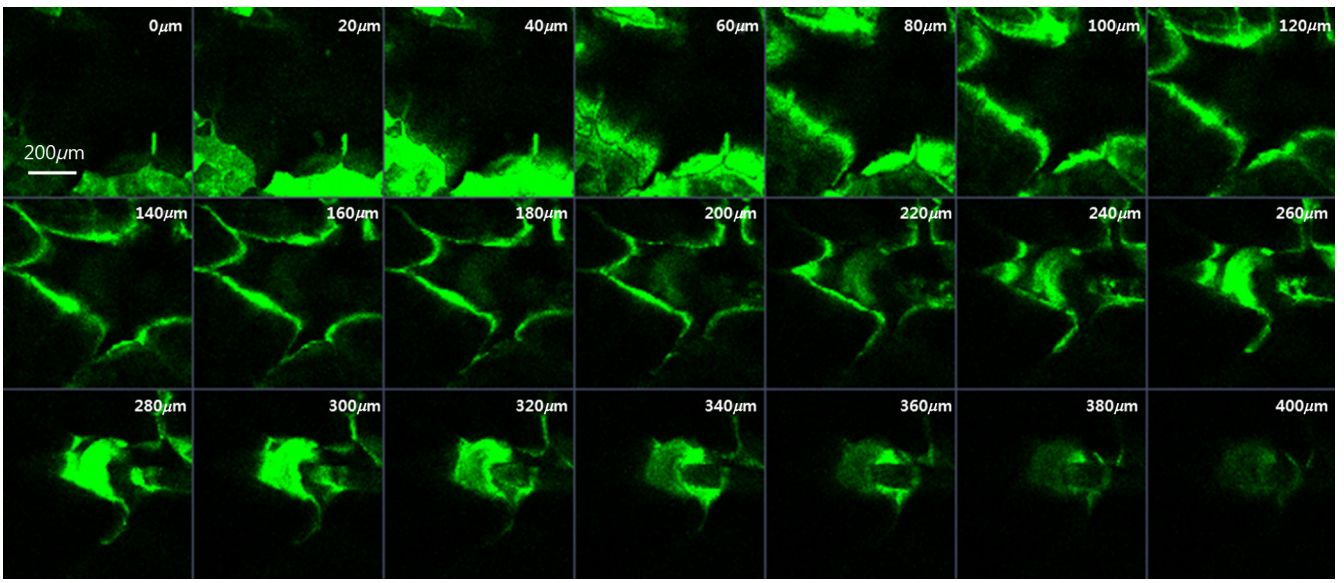

Fig. 8 Confocal microscopy image of penetration of porcine abdominal skin with fluorescein isothiocyanate (FITC) (microjet-only).

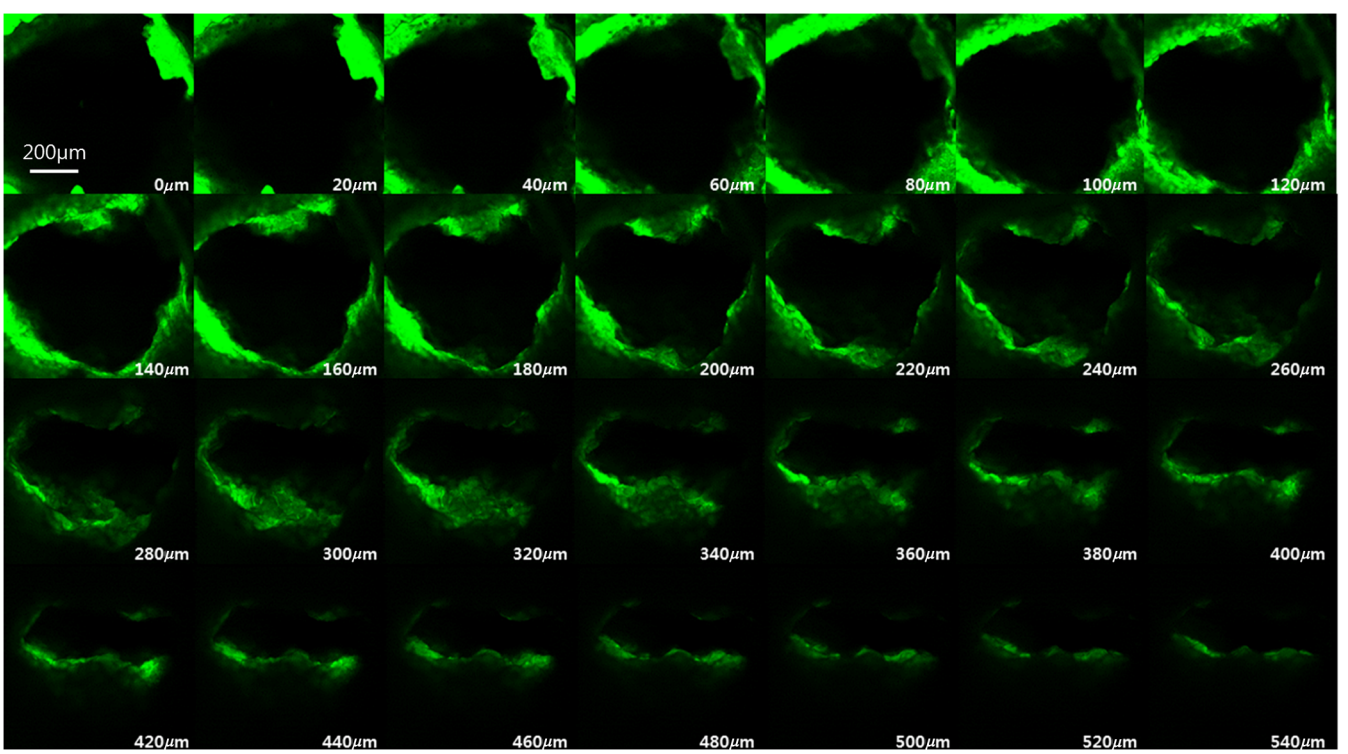

Fig. 9 Confocal microscopy image of penetration of porcine abdominal skin with FITC (preablation–microjet).

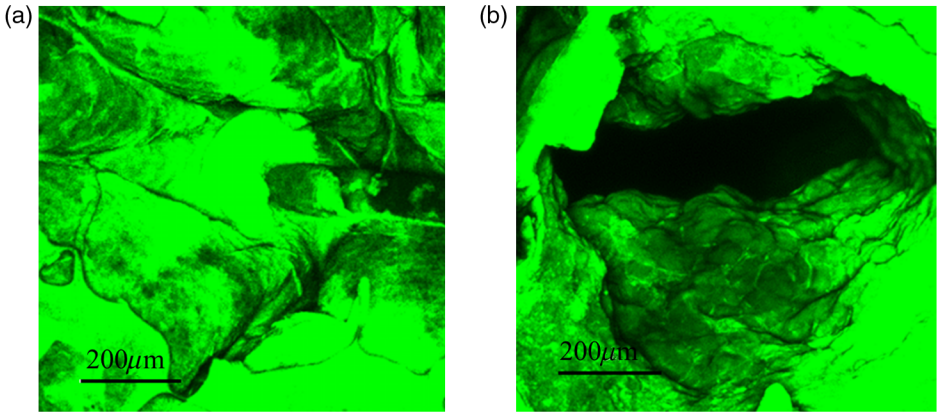

Fig. 10 Merged confocal microscopy image of (a) microjet-only case and (b) preablation–microjet case.

PAAG varies from 0.06 to 0.38 MPa, which is applicable to soft tissue phantoms.[14] The penetration depth and the injected volume are obtained from the images from gel tests, and are illustrated in Fig. 5 and Table 2. Each error bar is measured through a repeated injection of 10 times. For the microjet-only case, the penetration depth per energy decreased with the gel strength while the effect of the gel strength is not significant in the preablation–microjet case. This trend is more visible in Fig. 5(b) where the injected volumes for the ablation case are nearly constant regardless of the gel strength. Thus, the present combined scheme is an effective means of drug delivery for the target of varying skin strength.

The high speed camera images show that for the microjet-only case, the volume of injected ink has its maximum size at about 100 μs as shown in Fig. 6, which can be regarded as the equilibrium point between the expansive force of the jet and the restoring force of the gel. In the preablation–microjet case, shown in Fig. 7, laser ablation creates a hole before the microjet is injected. The jet speed in this case is 87.1 m/s, so the growth rate of the injected volume in the gel is slower than that of the microjet-only case.

The penetration experiment with abdominal porcine skin is also conducted to compare drug transfer efficiency. FITC (1 g/L) is dissolved in DPBS and injected into the skin to understand the depth of penetration and distribution of the delivered dose in the porcine epidermis (~0.5 mm below the outer layer). The number of repetitive injections is five times. Figure 8 shows the confocal microscopic images taken for the microjet-only case and Fig. 9 shows those of the preablation–microjet case. Each is a planar image taken at every 20-μm depth. The merged images of confocal microscopy for both cases are also provided in Fig. 10. In Fig. 8, a single hole in the center is seen with a good spread of the FITC stained tissue. The size of the hole becomes narrower with increasing penetration depth and the maximum depth reached by the staining solution is about

Table 3 Porcine skin test result on microjet injection w/ablation and w/o ablation.

	Penetration depth (μm)	Hole width (horizontal) (μm)	Hole width (vertical) (μm)
w/ablation	417 ± 108	679 ± 26	513 ± 129
w/o ablation	350 ± 71	614 ± 191	723 ± 42

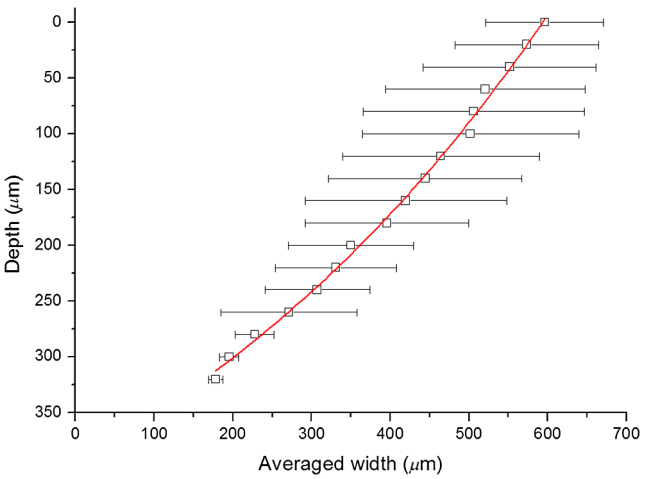

Fig. 11 Variation of skin penetration depth with varying hole width.

350 ± 71 μm as shown in Table 3. For the preablation–microjet case in Fig. 9, a hole created by a direct laser ablation is perceived. The staining agent penetrates right through this preablated spot (a microhole). The penetration depth in this case is larger and is 417 ± 108 μm, suggesting that preablation is quite useful. Even though the jet velocity is slower, a better drug delivery is attained by the combined preablation and microjet injection which also ensured a cleaner, deeper and softer drug passage (see Table 3).

The confocal images obtained from the repetitive experiments (repeated five times) are used to quantify the depth and width generated by the skin ablation. The width is measured at the center of both the horizontal and vertical axes. The values of the averaged maximum width of the horizontal and vertical axes are 679 ± 26 μm and 513 ± 129 μm, respectively. The shape of the hole is estimated from the variation in the averaged width with respect to the depth as shown in Fig. 11.

4 Conclusion

In this study, two different microjet injection schemes are considered. For the microjet-only case, the focused Er:YAG beam at a 150-μs pulse duration generates a strong vapor bubble inside the driving water chamber, which is responsible for ejecting a fast microjet of the intended drug solution. The efficiency of drug penetration into a porcine skin or PAAG depends on the

kinetic energy of the microjet. As for the preablation–microjet case, the same laser beam is split and 20% of the source is used to ablate a tiny spot on a skin before the remaining 80% energy driven microjet arrives at the preablated spot for an enhanced drug penetration. Both the kinetic energy of the microjet and the condition of the ablated skin are responsible for the noted enhancements.

Acknowledgments

We thank the Korea Research Foundation DOYAK-2010 (NRF-2010-0029125) and LG Household & Health Care for financial support through IAAT at Seoul National University. Authors also deeply acknowledge Mr. T. Hahn of Princeton University for useful discussion on the preablation concept for efficient microjet penetration into a porcine skin.

References

1. S. Mitragotri, "Current status and future prospects of needle-free liquid jet injectors," *Nat. Rev. Drug Discovery* **5**, 543–548 (2006).
2. J. C. Stachowiak, "Piezoelectric control of needle-free transdermal drug delivery," *J. Controlled Release* **124**, 88–97 (2007).
3. A. Taberner, N. C. Hogan, and I. W. Hunter, "Needle-free jet injection using real-time controlled linear Lorentz-force actuators," *Med. Eng. Phys.* **34**(9), 1228–1235 (2012).
4. D. A. Fletcher and D. V. Palanker, "Pulsed liquid microjet for micro-surgery," *Appl. Phys. Lett.* **78**(13), 1933–1935 (2001).
5. M. A. F. Kendall, "Needle-free vaccine injection," *Handb. Exp. Pharmacol.* **197**, 193–219 (2010).
6. M. R. Prausnitz and R. Langer, "Transdermal drug delivery," *Nat. Biotechnol.* **26**, 1261–1268 (2008).
7. M. Park et al., "Er:YAG laser pulse for small-dose splashback-free microjet transdermal drug delivery," *Opt. Lett.* **37**(18), 3894–3896 (2012).
8. H. Jang et al., "Towards clinical use of a laser-induced microjet system aimed at reliable and safe drug delivery," *J. Biomed. Opt.* **19**(5), 058001 (2014).
9. J. T. Walsh and T. F. Deutsch, "Er:YAG laser ablation of tissue: measurement of ablation rates," *Laser Surg. Med.* **9**, 327–337 (1989).
10. J. T. Walsh, T. J. Flotte, and T. F. Deutsch, "Er:YAG laser ablation of tissue: effect of pulse duration and tissue type on thermal damage," *Lasers Surg. Med.* **9**, 314–326 (1989).
11. R. Hibst and R. Kaufmann, "Effects of laser parameters on pulsed Er:YAG laser skin ablation," *Lasers Med. Sci.* **6**, 391 (1991).
12. U. Hohenleutner et al., "Fast and effective skin ablation with an Er:YAG laser: determination of ablation rates and thermal damage zones," *Lasers Surg. Med.* **20**, 242–247 (1997).
13. G. M. Hale and M. R. Querry, "Optical-constants of water in 200-nm to 200-μm wavelength region," *Appl. Opt.* **12**(3), 555–563 (1973).
14. J. S. Baxter, J. Katrencik, and S. Mitragotri, "Jet injection into polyacrylamide gels: investigation of jet injection mechanics," *J. Biomech.* **37**(8), 1181–1188 (2004).
15. U. Komaragiri, M. R. Begley, and J. G. Simmonds, "The mechanical response of freestanding circular elastic films under point and pressure loads," *J. Appl. Mech.* **72**(2), 203–212 (2005).

Biographies of the authors are not available.